

Numerical verification of random phase-and-amplitude formalism of weak turbulence

Mitsuhiro Tanaka*

Faculty of Engineering, Gifu University, Gifu 501-1193 Japan

Naoto Yokoyama†

Department of Aeronautics and Astronautics, Kyoto University, Kyoto 615-8540, Japan

(Dated: November 9, 2021)

The Random Phase and Amplitude Formalism (RPA) has significantly extended the scope of weak turbulence studies. Because RPA does not assume any proximity to the Gaussianity in the wavenumber space, it can predict, for example, how the fluctuation of the complex amplitude of each wave mode grows through nonlinear interactions with other modes, and how it approaches the Gaussianity. Thus, RPA has a great potential capability, but its validity has been assessed neither numerically nor experimentally. We compare the theoretical predictions given by RPA with the results of direct numerical simulation (DNS) for a three-wave Hamiltonian system, thereby assess the validity of RPA. The predictions of RPA agree quite well with the results of DNS in all the aspects of statistical characteristics of mode amplitudes studied here.

PACS numbers: 05.45.-a, 42.65.Wi, 47.27.-i

I. INTRODUCTION

In weak turbulence, wave trains which have different directions of the propagation, wavelengths, and frequencies weakly interact with each other owing to the nonlinearity in the governing equation and/or the boundary conditions. Many papers on weak turbulence have been devoted to the derivation of the kinetic equation [1–3], which governs the statistical evolution of the wave action spectrum, the physical and mathematical properties of the kinetic equation and resulting spectra [4–8], the statistically steady non-equilibrium spectra when the external forces and the dissipation balances [9, 10], and so on. Thus, researches on weak turbulence have been conventionally focused on the wave action spectrum, which is the ensemble average of the squared norm of the complex amplitude of each mode [11]. On the other hand, the spectra which are observed in the direct numerical simulations (DNS) and field observations have large fluctuations. In DNS, the amplitude of each wave mode is often determined by a prescribed spectrum and initially have no fluctuations at all. Even in such DNS, the amplitude fluctuations spontaneously grow as time elapses. The generation mechanism of the fluctuations, the time scales of their growths, and the possibility of the approach to the Gaussianity had little been studied.

The Random Phase and Amplitude Formalism (RPA) which has recently been developed has changed the situation, and drastically extended the scope of weak turbulence research [12–15]. Similar to the conventional weak turbulence theory, RPA is the statistical theory for the complex amplitude $a_{\mathbf{k}}$. Let $a_{\mathbf{k}}$ be expressed as $a_{\mathbf{k}} = |a_{\mathbf{k}}|\psi_{\mathbf{k}}$ with the positive amplitude $|a_{\mathbf{k}}|$ and the

phase factor $\psi_{\mathbf{k}} = e^{i\phi_{\mathbf{k}}}$. In the Random Phase approximation (RP) in the strict sense, it is assumed that $\psi_{\mathbf{k}}$ for all \mathbf{k} are independent random variables and are uniformly distributed over the unit circle in the complex plane. In the Random Phase and Amplitude Formalism it is assumed, in addition to the assumptions of RP, that the amplitude $|a_{\mathbf{k}}|$ also are mutually independent random variables for all \mathbf{k} . It is important to note that in RPA $|a_{\mathbf{k}}|$ is allowed to have any distribution and can be far from the Gaussianity. Although it is only recently that RPA is defined unambiguously, it has implicitly been used for a rather long time under the name of “the random phase approximation”, often without being realized of it. For example, Zakharov et al. ([11]p.65) calls their approximation “the random phase approximation”, but they implicitly assume the statistical independence of the amplitude $|a_{\mathbf{k}}|$ for different \mathbf{k} .

The equations which describe the time evolution of the moments of $|a_{\mathbf{k}}|^2$ for arbitrary orders as well as the probability density function (PDF) of $|a_{\mathbf{k}}|^2$ have been derived. Thus, RPA is expected to describe the statistical characteristics of the amplitude fluctuations, which have little been studied. Although RPA seems to have a great potential capability, its validity has been assessed neither numerically nor experimentally. In this study, we perform a series of large-scale DNS for a model Hamiltonian system which allows three-wave resonance, and compare the results with the theoretical predictions of RPA. Here we confine our attention to the single-mode statistics of the amplitude fluctuations. In every aspect studied here, we have obtained good quantitative agreement between RPA and DNS.

Benney and Newell [16] investigated the n th order cumulant $R^{(n)}$ of a wave turbulence field in the physical space, and derived an equation which governs the temporal evolution of the Fourier transform of $R^{(n)}$. They assumed that the wave field is weak nonlinear and that the medium is dispersive, but did not assume that the wave

* tanaka@gifu-u.ac.jp

† yokoyama@kuaero.kyoto-u.ac.jp

field is close to a Gaussian state in the physical space. Prior to [16], Benney and Saffman [17] derived the kinetic equation for the action spectrum based on the same assumptions. In the present paper, we will compare our numerical results with the predictions of RPA only, and will not try any comparison with the predictions of [16] mainly from the following two reasons. Firstly, [16] is described in terms of the Fourier transform of a real-valued physical variable, and it is not expressed in terms of the complex amplitude of wave modes which we want to handle. Secondly, [16] does not introduce the discretization of the \mathbf{k} space and the Fourier transform is a generalized function. On the other hand, RPA treats the discretized \mathbf{k} space from the outset, hence the comparison with DNS is straightforward and much easier than the case of [16]. There is also an essential difference between RPA and the analysis in [16],[17] with regard to the speed of decay of the correlations in the physical space as functions of the separation of points. (See for example [12].)

This paper is organized as follows. The numerical

scheme is presented in Sec. II. In Sec. III, numerical results of the evolution of the amplitude fluctuations and the approach to the Gaussianity are reported. The discussion and the summary are given in Sec. IV.

II. NUMERICAL SCHEME

A. Numerical Model

In this study we employ the following three-wave Hamiltonian system:

$$\mathcal{H} = \mathcal{H}_2 + \mathcal{H}_3, \quad (1a)$$

$$\mathcal{H}_2 = \int \omega(\mathbf{k}) |a(\mathbf{k})|^2 d\mathbf{k}, \quad (1b)$$

$$\begin{aligned} \mathcal{H}_3 = \frac{1}{2} \int (V(\mathbf{k}, \mathbf{k}_1, \mathbf{k}_2) a^*(\mathbf{k}) a(\mathbf{k}_1) a(\mathbf{k}_2) + \text{c.c.}) \\ \times \delta(\mathbf{k} - \mathbf{k}_1 - \mathbf{k}_2) d\mathbf{k}_{123}. \end{aligned} \quad (1c)$$

$$\begin{aligned} \frac{da(\mathbf{k})}{dt} &= -i \frac{\delta \mathcal{H}}{\delta a^*(\mathbf{k})} \\ &= -i\omega(\mathbf{k})a(\mathbf{k}) \\ &\quad - \frac{i}{2} \int V(\mathbf{k}, \mathbf{k}_1, \mathbf{k}_2) a(\mathbf{k}_1) a(\mathbf{k}_2) \delta(\mathbf{k} - \mathbf{k}_1 - \mathbf{k}_2) d\mathbf{k}_{12} - i \int V^*(\mathbf{k}_1, \mathbf{k}, \mathbf{k}_2) a(\mathbf{k}_1) a^*(\mathbf{k}_2) \delta(\mathbf{k}_1 - \mathbf{k} - \mathbf{k}_2) d\mathbf{k}_{12}, \end{aligned} \quad (2a)$$

$$\omega(\mathbf{k}) = k^\alpha, \quad V(\mathbf{k}, \mathbf{k}_1, \mathbf{k}_2) = (kk_1k_2)^\beta, \quad \alpha = 3/2, \quad \beta = 1/4. \quad (2b)$$

Here, \mathbf{k} is a two-dimensional wavenumber vector, a^* expresses the complex conjugate of a , and c.c. also expresses the complex conjugate of the preceding term. The linear frequency and the complex amplitude of the mode of the wavenumber \mathbf{k} are respectively expressed by $\omega(\mathbf{k})$ and $a(\mathbf{k})$. The short-hand notations $k = |\mathbf{k}|$ and $d\mathbf{k}_{12} = d\mathbf{k}_1 d\mathbf{k}_2$ are used. When we derive the dynamic equations for the complex amplitude in weak turbulence systems, we often obtain the dynamic equation like Eq. (2a) when the three-wave resonant interactions are allowed like in the surface capillary waves [11]. In fact, the difference between the dynamic equation for surface capillary waves and that for our model appears only in the interaction kernel $V(\mathbf{k}, \mathbf{k}_1, \mathbf{k}_2)$. For our objective to generally compare DNS with RPA, we select the simple interaction kernel that allows the evaluation of the convolution in the nonlinear terms to be performed fast by the Fast Fourier Transforms (FFT).

In numerical studies of weak turbulence, one sometimes adds artificial energy input and/or output to the conservative system (2a). If we were to investigate weak turbulence characteristics in a statistically steady state,

such as the Kolmogorov–Zakharov spectrum, it would be necessary to add such non-conservative effects. On the other hand, the purpose of the present study is to assess the validity of the prediction of RPA on the temporal evolution of various statistics of $a_{\mathbf{k}}$. Therefore, we need statistical unsteadiness of the wave field, and in this respect the conservative system without input or output is in accord to our purpose as it stands.

B. Correspondence between Continuous System and Discrete System

Some cautions should be exercised when we compare the theoretical description where the wavenumbers are continuous with numerical results where the wavenumbers are discrete. To connect the wavenumber space and the real space, we select the definition of the Fourier

transform as follows:

$$f(\mathbf{x}) = \frac{1}{2\pi} \int F(\mathbf{k}) e^{i\mathbf{k}\cdot\mathbf{x}} d\mathbf{k}, \quad F(\mathbf{k}) = \frac{1}{2\pi} \int f(\mathbf{x}) e^{-i\mathbf{k}\cdot\mathbf{x}} d\mathbf{x}, \quad (3)$$

where \mathbf{x} is a two-dimensional vector in the real space. We also select the Fourier series which connects the rectangular domain $R = L_x \times L_y$ in the real space under the doubly periodic boundary conditions to the discrete wavenumber \mathbf{k} :

$$f(\mathbf{x}) = \sum_{\mathbf{k} \in S_k} F_{\mathbf{k}} e^{i\mathbf{k}\cdot\mathbf{x}}, \quad F_{\mathbf{k}} = \frac{1}{L_x L_y} \int_R f(\mathbf{x}) e^{-i\mathbf{k}\cdot\mathbf{x}} d\mathbf{x}, \quad (4)$$

where S_k is a set of \mathbf{k} allowed in the discrete wavenumber space, i.e.,

$$S_k = \{\mathbf{k} \mid \mathbf{k} = (m\Delta k_x, n\Delta k_y), (m, n) \in \mathbb{Z}^2\}. \quad (5)$$

The grid intervals in the discrete wavenumbers Δk_x and Δk_y are connected to the periods in the real space L_x and L_y as

$$\Delta k_x = \frac{2\pi}{L_x}, \quad \Delta k_y = \frac{2\pi}{L_y}. \quad (6)$$

Because of the properties of the delta function

$$\delta(\mathbf{k}) = \frac{1}{(2\pi)^2} \int e^{i\mathbf{k}\cdot\mathbf{x}} d\mathbf{x}, \quad (7)$$

and of the Kronecker's delta for $\mathbf{k} \in S_k$

$$\delta_{\mathbf{k}, \mathbf{0}} = \frac{1}{L_x L_y} \int_R e^{i\mathbf{k}\cdot\mathbf{x}} d\mathbf{x} = \frac{\Delta k_x \Delta k_y}{(2\pi)^2} \int_R e^{i\mathbf{k}\cdot\mathbf{x}} d\mathbf{x}, \quad (8)$$

the correspondence

$$\delta(\mathbf{k}) \longleftrightarrow \frac{1}{\Delta k_x \Delta k_y} \delta_{\mathbf{k}, \mathbf{0}} \quad (9)$$

is found for sufficiently small Δk_x and Δk_y .

Because of the relation between $F(\mathbf{k})$ and $F_{\mathbf{k}}$ which generally holds

$$F(\mathbf{k}) = \sum_{\mathbf{k}' \in S_k} 2\pi F_{\mathbf{k}'} \delta(\mathbf{k} - \mathbf{k}'), \quad (10)$$

and the correspondence (9), the following correspondence is found:

$$a(\mathbf{k}) \longleftrightarrow \frac{2\pi}{\Delta k_x \Delta k_y} a_{\mathbf{k}}, \quad (11)$$

for $\mathbf{k} \in S_k$.

The wave actions, $n(\mathbf{k})$ for the continuous system and $n_{\mathbf{k}}$ for the discrete system, are respectively defined as

$$n(\mathbf{k}) \delta(\mathbf{k} - \mathbf{k}') = \langle a(\mathbf{k}) a^*(\mathbf{k}') \rangle \text{ and } n_{\mathbf{k}} \delta_{\mathbf{k}, \mathbf{k}'} = \langle a_{\mathbf{k}} a_{\mathbf{k}'}^* \rangle, \quad (12)$$

where $\langle \dots \rangle$ represents the ensemble average. The correspondences (9) and (11) give the correspondence of the wave actions

$$n(\mathbf{k}) \longleftrightarrow \frac{(2\pi)^2}{\Delta k_x \Delta k_y} n_{\mathbf{k}}. \quad (13)$$

The governing equation in the discretized wavenumbers corresponding to Eq. (2a) is written as

$$\begin{aligned} \frac{da_{\mathbf{k}}}{dt} = & -i\omega_{\mathbf{k}} a_{\mathbf{k}} - \frac{i}{2} (2\pi) \sum_{\mathbf{k}_1, \mathbf{k}_2} V_{\mathbf{k}_1 \mathbf{k}_2}^{\mathbf{k}} a_{\mathbf{k}_1} a_{\mathbf{k}_2} \delta_{\mathbf{k}_1 \mathbf{k}_2}^{\mathbf{k}} \\ & - i(2\pi) \sum_{\mathbf{k}_1, \mathbf{k}_2} V_{\mathbf{k} \mathbf{k}_2}^{\mathbf{k}_1} a_{\mathbf{k}_1} a_{\mathbf{k}_2}^* \delta_{\mathbf{k} \mathbf{k}_2}^{\mathbf{k}_1}, \end{aligned} \quad (14)$$

where $\omega_{\mathbf{k}} = \omega(\mathbf{k})$, $V_{\mathbf{k}_1 \mathbf{k}_2}^{\mathbf{k}} = V(\mathbf{k}, \mathbf{k}_1, \mathbf{k}_2)$, and $\delta_{\mathbf{k}_1 \mathbf{k}_2}^{\mathbf{k}}$ expresses the Kronecker's delta $\delta_{\mathbf{k}, \mathbf{k}_1 + \mathbf{k}_2}$. Note that, in addition that the integration and the delta function are respectively replaced by the summation and the Kronecker's delta, the quadratic nonlinear terms have the coefficient 2π .

C. Configuration of Numerical Simulations

In our numerical simulations the wavenumber space $\mathbf{k} = (k_x, k_y)$ is discretized by the equally-distributed grids with the interval $\Delta k = 1/42$ in both k_x and k_y directions and is truncated along $|k_x| = k_{\max}$ and $|k_y| = k_{\max}$ with $k_{\max} = 512\Delta k \approx 12$. The convolutions in the nonlinear terms are obtained by the pseudospectral transform method. In this method we first use inverse FFT of size $n_x = n_y = 1024$ to transform $a_{\mathbf{k}}$ to its inverse transform in the physical \mathbf{x} space, perform there suitable multiplications, and then use the FFT to obtain the convolution sums. Although this pseudospectral transform method contains the aliasing error, the region $|k_x|, |k_y| \leq 341\Delta k \approx 8$ in the \mathbf{k} space is free from this aliasing error due to the 3/2-rule. (For the 3/2-rule, see for example [18].) We trace the temporal evolutions of $a_{\mathbf{k}}$ only for those \mathbf{k} 's which are within this alias-free region.

By reference to the Pierson-Moskowitz spectrum that is typical in the ocean waves, we employ an isotropic spectrum as follows for the initial wave field:

$$H_2 = \sum_{\mathbf{k}} \omega_{\mathbf{k}} |a_{\mathbf{k}}|^2, \quad (15a)$$

$$|a_{\mathbf{k}}|^2 = A k^{-6.5} \exp(-1/k^4) D(k), \quad (15b)$$

$$D(k) = \begin{cases} 1, & (0 < k < 7), \\ \exp(-10(k-7)^2), & (7 \leq k \leq 8), \end{cases} \quad (15c)$$

where H_2 is the discrete counterpart of the lowest-order Hamiltonian \mathcal{H}_2 of (1b). The exponential function and the power-law function in Eq. (15b) respectively give the increase in the small wavenumbers and the decrease in the large wavenumbers. The function $D(k)$ gives the exponential tail near the end of the alias-free wavenumbers so that the truncation in the \mathbf{k} space does not affect

the numerical results. For the purpose of this study the choice of the spectrum is arbitrary, and this spectrum (15) does not have any special significance for the system at all. Here, the coefficient A is a parameter to control the value of H_2 . In this study, we performed four series of simulations which have $H_2 = 1.25 \times 10^{-6}$, 2.5×10^{-6} , 5×10^{-6} , and 1×10^{-5} . The initial phases of each component wave are given by uniform random numbers in the range $[0, 2\pi]$. The ratio $|H_3/H_2|$ can be a measure of the degree of nonlinearity of the wave field as a whole, where H_3 is the discrete counterpart of the interaction Hamiltonian \mathcal{H}_3 of (1c). $|H_3/H_2|$ is an increasing function of H_2 , and takes values around 5.0×10^{-5} when $H_2 = 1.25 \times 10^{-6}$ and 3.5×10^{-4} when $H_2 = 1 \times 10^{-5}$. Our selection of the values of H_2 as above is made to keep $|H_3/H_2|$ and hence the nonlinearity of the wave field sufficiently small. To make ensemble average, 256 independent simulations which have the different initial phases are performed for each H_2 . The time integration is made until $t = 100T_p$. Here, $T_p = 2\pi$ is the period given by the linear dispersion relation for $k = 1$, at which the one-dimensional energy spectrum defined below has its maximum. The fourth-order Runge-Kutta method with the time interval $\Delta t = T_p/50$ is employed for the time integration. The linear term is implicitly solved to improve the numerical stability. Because the system and the initial spectrum are isotropic, $a_{\mathbf{k}}$ for $k > 8$ is set to 0 at each time step.

The total Hamiltonian that is the sum of the linear part H_2 and the nonlinear part H_3 is numerically conserved within the relative error 2.6×10^{-4} for $H_2 = 1 \times 10^{-5}$ where the nonlinearity is the largest and the conservation is the worst. In this case, the average of H_3 during $100T_p$ is -3.5×10^{-9} .

All the numerical simulations are performed on FUJITSU FX1 in Information Technology Center, Nagoya University. The CPU time for one realization takes 12

hours.

III. NUMERICAL RESULTS

A. Time Evolution of Spectra

Figure 1 shows the azimuthally-integrated one-dimensional energy spectra $E(k)$

$$E(k) = \frac{1}{\Delta_{\text{bin}}} \sum_{k - \Delta_{\text{bin}}/2 < |\mathbf{k}'| < k + \Delta_{\text{bin}}/2} \langle \omega_{\mathbf{k}'} | a_{\mathbf{k}'}|^2 \rangle, \quad (16)$$

obtained from DNS at $t = 100T_p$. The initial spectra are also shown for reference. Here, Δ_{bin} denotes the width of the bins which is used to evaluate $E(k)$ from the complex amplitudes defined on the discrete wavenumbers, and we set $\Delta_{\text{bin}} = 0.05$. Figures 1 (a), (b), (c) and (d) show the energy spectra for $H_2 = 1.25 \times 10^{-6}$, for $H_2 = 2.5 \times 10^{-6}$, for $H_2 = 5 \times 10^{-6}$, and for $H_2 = 1 \times 10^{-5}$, respectively. Small irregularities around $k = 1.1$ are due to the numerical procedures to obtain $E(k)$ in the discrete \mathbf{k} space. While the variation of the spectrum during $100T_p$ for $H_2 = 1.25 \times 10^{-6}$ is quite small, that for $H_2 = 1 \times 10^{-5}$ is large during the time. Most of the weak turbulence theory, including RPA studied here, have been developed for the *weak* turbulence, where the linear time scale determined by the linear frequency and the nonlinear time scale, i.e., the time scale of spectral change are largely separated. Therefore, the weakly nonlinear assumption might be slightly violated for $H_2 = 1 \times 10^{-5}$, although the assumption is evidently valid for $H_2 = 1.25 \times 10^{-6}$.

The wave action $n(\mathbf{k})$ of the three-wave system (2) is known to evolve according to the following kinetic equation (See, for example, Refs. [11, 13]):

$$\frac{dn(\mathbf{k})}{dt} = -\gamma(\mathbf{k})n(\mathbf{k}) + \eta(\mathbf{k}), \quad (17a)$$

$$\eta(\mathbf{k}) = \pi \int \left(|V(\mathbf{k}, \mathbf{k}_1, \mathbf{k}_2)|^2 \delta(\mathbf{k} - \mathbf{k}_1 - \mathbf{k}_2) \delta(\omega(\mathbf{k}) - \omega(\mathbf{k}_1) - \omega(\mathbf{k}_2)) \right. \\ \left. + 2 |V(\mathbf{k}_2, \mathbf{k}, \mathbf{k}_1)|^2 \delta(\mathbf{k}_2 - \mathbf{k} - \mathbf{k}_1) \delta(\omega(\mathbf{k}_2) - \omega(\mathbf{k}) - \omega(\mathbf{k}_1)) \right) n_{\mathbf{k}_1} n_{\mathbf{k}_2} d\mathbf{k}_{12}, \quad (17b)$$

$$\gamma(\mathbf{k}) = 2\pi \int \left(|V(\mathbf{k}, \mathbf{k}_1, \mathbf{k}_2)|^2 \delta(\mathbf{k} - \mathbf{k}_1 - \mathbf{k}_2) \delta(\omega(\mathbf{k}) - \omega(\mathbf{k}_1) - \omega(\mathbf{k}_2)) n(\mathbf{k}_2) \right. \\ \left. + |V(\mathbf{k}_2, \mathbf{k}, \mathbf{k}_1)|^2 \delta(\mathbf{k}_2 - \mathbf{k} - \mathbf{k}_1) \delta(\omega(\mathbf{k}_2) - \omega(\mathbf{k}) - \omega(\mathbf{k}_1)) (n(\mathbf{k}_2) - n(\mathbf{k}_1)) \right) d\mathbf{k}_{12}. \quad (17c)$$

Since the energy spectrum for $H_2 = 1.25 \times 10^{-6}$ varies very little during the time $100T_p$ as shown in Fig. 1(a), the right hand side of Eq. (17a) is almost constant in time and the wave action is expected to be a linear function of time. Figure 2 shows the time rates of change

of $E(k)$ for $H_2 = 1.25 \times 10^{-6}$. One is obtained for the initial spectrum (15) according to Eq. (17). The other is obtained from DNS as the difference between the energy spectrum at $t = 50T_p$ and that at $t = 0$ divided by $50T_p$. Both time rates of change agree quite well.

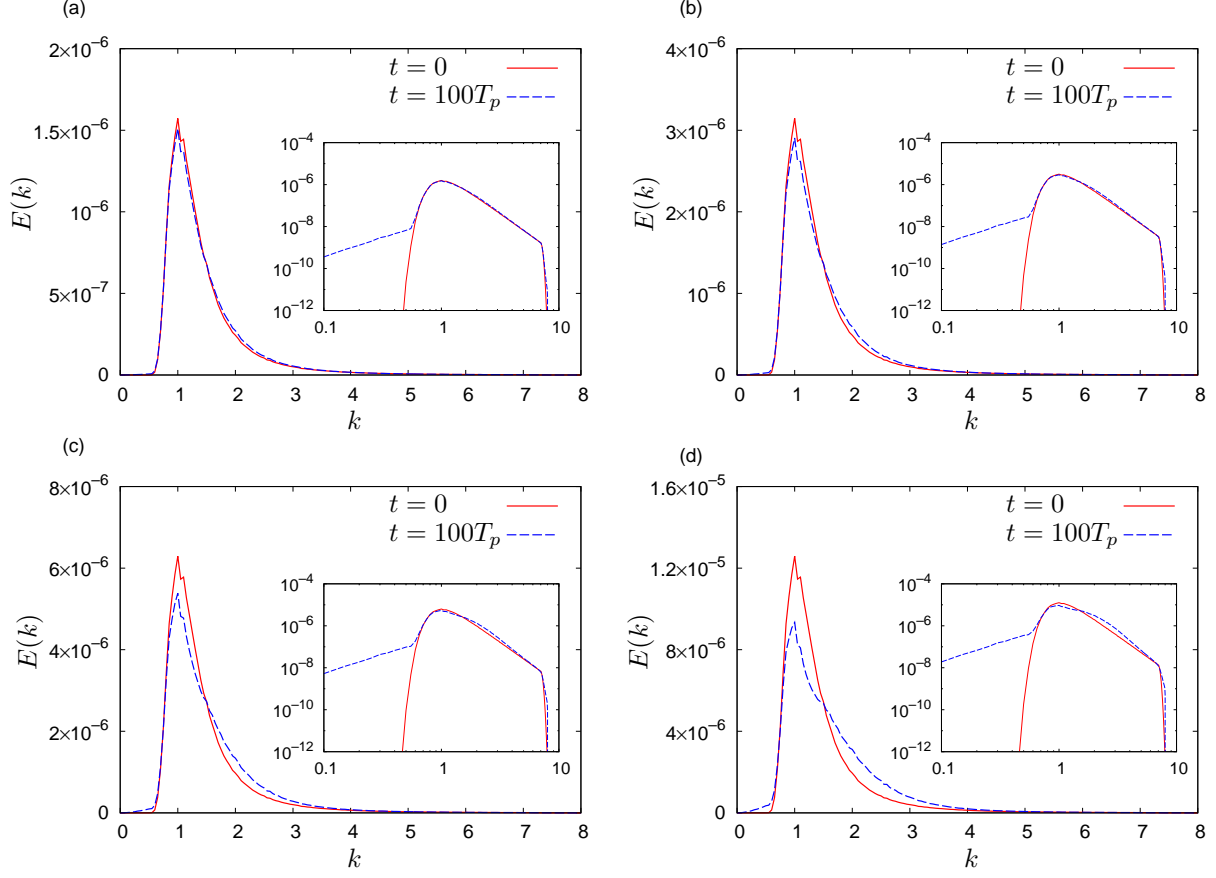


FIG. 1. (Color online) Variations of one-dimensional energy spectra $E(k)$ from $t = 0$ to $t = 100T_p$. The spectra are shown with the double logarithmic scales in the insets. (a): $H_2 = 1.25 \times 10^{-6}$, (b): $H_2 = 2.5 \times 10^{-6}$, (c): $H_2 = 5 \times 10^{-6}$, (d): $H_2 = 1 \times 10^{-5}$.

The same procedure of the comparison cannot be used for $H_2 = 1 \times 10^{-5}$, since the variation of $E(k)$ is large. Then, the energy spectrum at $100T_p$ is obtained by the numerical integration of Eq. (17) in time, and it is compared with the energy spectrum at $t = 100T_p$ obtained by DNS, which is already shown in Fig. 1(d). The comparison is shown in Fig. 3. Also for $H_2 = 1 \times 10^{-5}$, both spectra agree quite well. It clearly shows that the spectrum in DNS evolves in time according to the prediction of the kinetic equation (17).

B. Importance of Resonant Interaction for Evolution of Fluctuation

In our DNS, the initial value of the amplitude of each wave mode $|a_{\mathbf{k}}(0)|$ is determined by the initial spectrum, hence no amplitude fluctuation exists at $t = 0$. The fluctuation grows as time elapses through nonlinear interactions with other modes. Examples of the evolution of $|a_{\mathbf{k}}|^2$ are shown in Fig. 4. The five curves show the variations of $|a_{\mathbf{k}}|^2$ for $\mathbf{k} = (3, 0)$ in five independent realizations for $H_2 = 5 \times 10^{-6}$. Since the simulations are

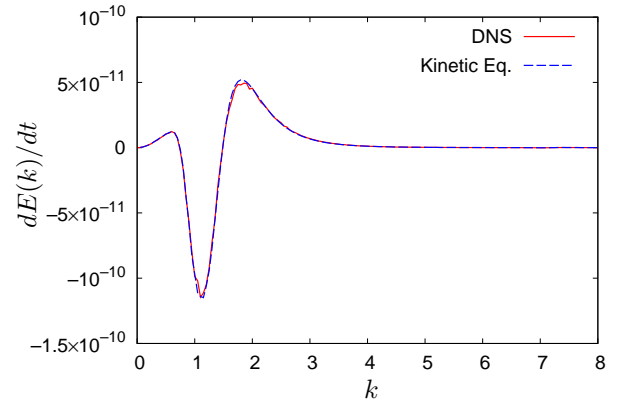


FIG. 2. (Color online) Comparison of the time rates of change of $E(k)$ between DNS and the kinetic equation. $H_2 = 1.25 \times 10^{-6}$.

started without the amplitude fluctuations, all $|a_{\mathbf{k}}|^2$ has the same value at $t = 0$. The fluctuations grow as time elapses, and each $|a_{\mathbf{k}}|^2$ evolves differently.

Figure 5 shows the time evolutions of the mean $n_{\mathbf{k}}$

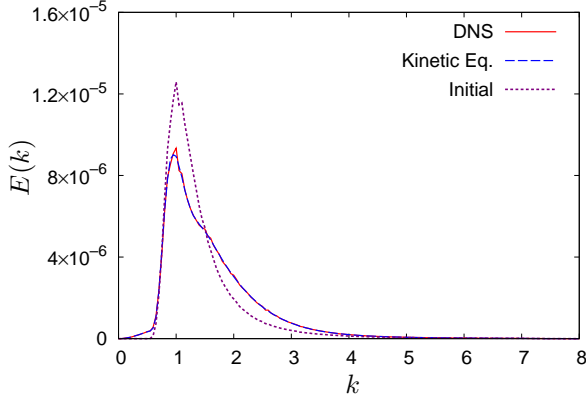


FIG. 3. (Color online) Comparison of the variations of $E(k)$ from $t = 0$ to $t = 100T_p$ between DNS and the kinetic equation. $H_2 = 1 \times 10^{-5}$.

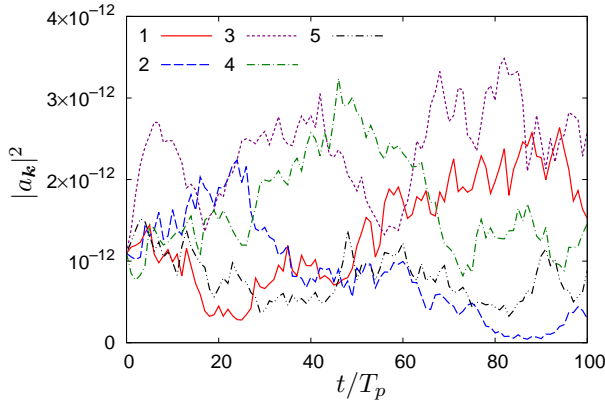


FIG. 4. (Color online) Evolution of $|a_{\mathbf{k}}|^2$ in five independent realizations. $H_2 = 5 \times 10^{-6}$, $\mathbf{k} = (3, 0)$.

and the standard deviation $\sigma_{\mathbf{k}}$ of $|a_{\mathbf{k}}|^2$ obtained from DNS for $H_2 = 5 \times 10^{-6}$. Figures 5 (a), (b), (c) and (d) respectively show the evolution of $n_{\mathbf{k}}$ and $\sigma_{\mathbf{k}}$ of $k = 1$, $k = 1.5$, $k = 3$ and $k = 6$. Throughout this paper, to evaluate the statistical quantities at k such as $n_{\mathbf{k}}$, the quantity is averaged over the modes of \mathbf{k}' in the annular domain $|k - k'| < \Delta_{\text{bin}}/2 (= 0.025)$. It can be seen that $\sigma_{\mathbf{k}}$, that is, the amplitude fluctuation grows in time at each k , although the growth rates are wavenumber-dependent. In particular, at the larger wavenumbers $k = 3$ and $k = 6$, it is clearly observed that the fluctuations are approaching the Gaussianity of $a_{\mathbf{k}}$, i.e., $n_{\mathbf{k}} = \sigma_{\mathbf{k}}$.

For comparison, we performed another series of DNS where the power-law exponent α of the linear dispersion relation in Eq. (2b) is changed to $\alpha = 1/2$ while all the other aspects of the model remain intact. In this case, the dispersion relation $\omega = k^{1/2}$ is of non-decay type, which is similar to the surface gravity waves in water, and the three-wave resonant interactions are prohibited. The results are shown in Fig. 6 where we draw the same quantities shown in Figs. 4 and 5(c). By comparing Fig. 6

with Figs. 4 and 5(c), we observe that the growth of the fluctuations is much slower when the three-wave resonant interactions are prohibited by the dispersion relation. Similarly, the slower growths are observed for other wavenumbers.

The kinetic equation (17) derived by the weak turbulence theory represents that only the resonant interactions play a role in the evolution of the wave action $n_{\mathbf{k}}$. It can simply be understood since the secular energy transfer persistent against the time average is necessary for $n_{\mathbf{k}}$, which is the mean of $|a_{\mathbf{k}}|^2$, to evolve and only the resonant interactions can provide it. On the other hand, the fluctuations of $|a_{\mathbf{k}}|^2$ around its mean could grow owing to the non-resonant nonlinear interactions as well as the resonant ones, for the non-resonant interactions seem to work as the stochastic driving forces in random walk processes. Against the intuition, however, the comparison between Figs. 4 and 5 and Fig. 6 clearly shows that the resonant interactions are essential for the evolution of the fluctuations. Even though the three-wave resonances are prohibited when $\alpha = 1/2$ and our model (2a) contains only quadratic nonlinear terms, the fluctuations do grow as shown in Fig. 6(b) albeit very slowly. This is because two non-resonant three-wave interactions can make a resonant four-wave interaction, and hence the fluctuations grow due to this four-wave resonant interaction with a much slower time scale.

C. Approach to Gaussianity

The p th-order moment is defined as

$$M^{(p)}(\mathbf{k}) = \left\langle \left(\frac{|a(\mathbf{k})|^2}{\delta(\mathbf{0})} \right)^p \right\rangle, \quad (18)$$

where $\delta(\mathbf{0})$ is defined in the large-box limit as

$$\delta(\mathbf{0}) = \lim_{L_x, L_y \rightarrow \infty} \frac{L_x L_y}{(2\pi)^2} = \lim_{\Delta k_x, \Delta k_y \rightarrow 0} \frac{1}{\Delta k_x \Delta k_y}, \quad (19)$$

according to the correspondence (9). RPA predicts that $M^{(p)}(\mathbf{k})$ evolves according to the following equation [14]:

$$\frac{dM^{(p)}(\mathbf{k})}{dt} = -p\gamma(\mathbf{k})M^{(p)}(\mathbf{k}) + p^2\eta(\mathbf{k})M^{(p-1)}(\mathbf{k}), \quad (20)$$

where $\eta(\mathbf{k})$ and $\gamma(\mathbf{k})$ are respectively given in Eq. (17b) and Eq. (17c). Equation (20) for $p = 1$ is identical to the kinetic equation (17) for the wave action $n(\mathbf{k})$.

When the real and imaginary parts of $a(\mathbf{k})$ are independent and obey the same Gaussian distribution,

$$M^{(p)}(\mathbf{k}) = p! n^p(\mathbf{k}). \quad (21)$$

Then,

$$F^{(p)}(\mathbf{k}) = \frac{M^{(p)}(\mathbf{k}) - p! n^p(\mathbf{k})}{p! n^p(\mathbf{k})}, \quad (22)$$

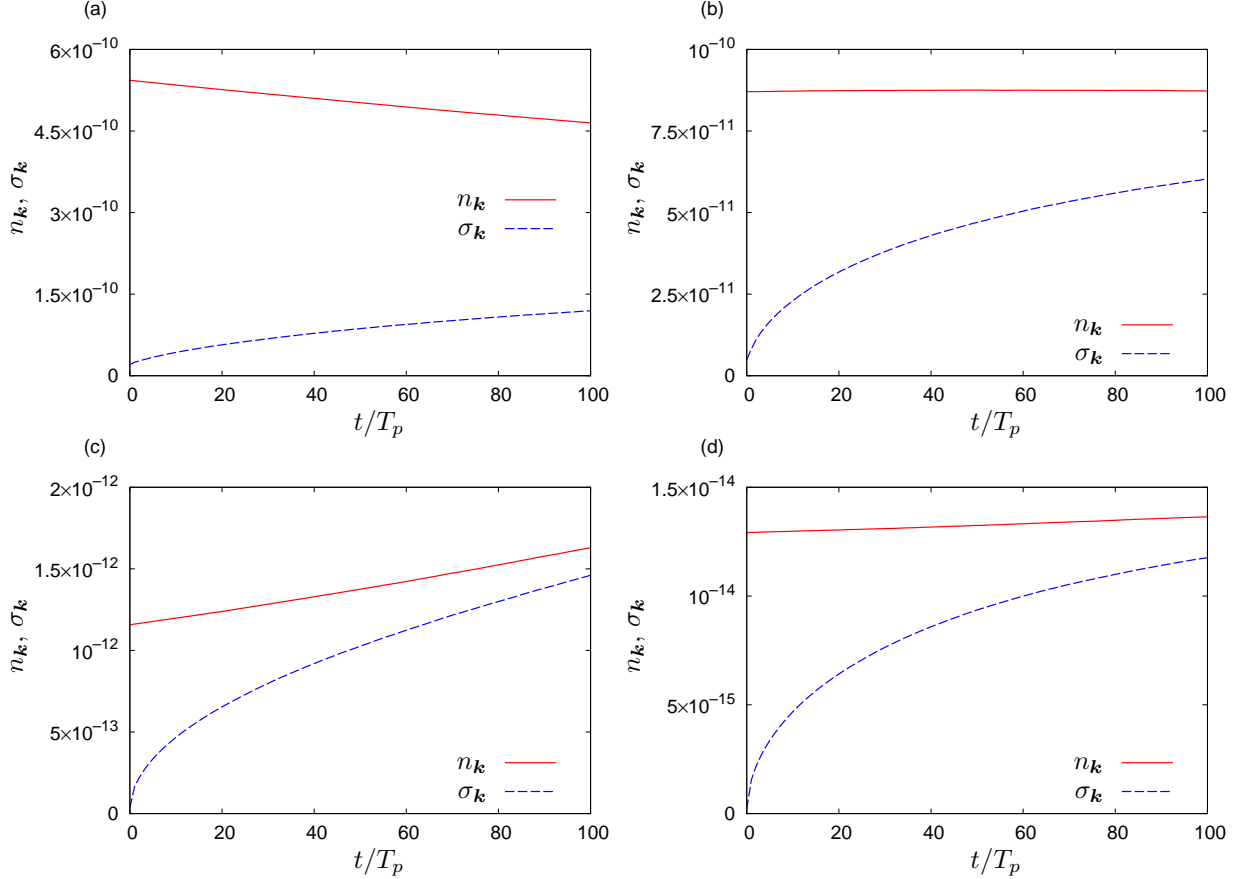


FIG. 5. (Color online) Evolution of the means $n_{\mathbf{k}}$ and the standard deviations $\sigma_{\mathbf{k}}$ of $|a_{\mathbf{k}}|^2$. $H_2 = 5 \times 10^{-6}$. (a): $k = 1$, (b): $k = 1.5$, (c): $k = 3$, (d): $k = 6$.

is an index which expresses the deviation from the Gaussianity of $a(\mathbf{k})$. Equation (20) can be written for $F^{(p)}(\mathbf{k})$ as

$$\frac{dF^{(p)}(\mathbf{k})}{dt} = \frac{p\eta(\mathbf{k})}{n(\mathbf{k})} \left(F^{(p-1)}(\mathbf{k}) - F^{(p)}(\mathbf{k}) \right). \quad (23)$$

Because $F^{(1)}(\mathbf{k}) = 0$ by the definition that $M^{(1)}(\mathbf{k}) = n(\mathbf{k})$, the equation for the evolution of $F^{(2)}(\mathbf{k})$ can be obtained as

$$\frac{dF^{(2)}(\mathbf{k})}{dt} = -\frac{2\eta(\mathbf{k})}{n(\mathbf{k})} F^{(2)}(\mathbf{k}). \quad (24)$$

When $|a(\mathbf{k})|$ is deterministically given and no fluctuation is allowed like in the initial conditions of our DNS, $F^{(2)}(\mathbf{k}) = -1/2$. Equation (23) represents that the deviation from the Gaussianity of $a(\mathbf{k})$ for all p decays after the elapse of sufficient time, because $\eta(\mathbf{k}) > 0$. The homogeneous term in Eq. (23) indicates that $F^{(p)}(\mathbf{k})$ for large p decays fast, and then the non-homogeneous term of the order $p - 1$ can be dominant in the evolution of $F^{(p)}(\mathbf{k})$. Therefore, the evolution of $F^{(p)}(\mathbf{k})$ for all p is determined by the slowest $F^{(2)}(\mathbf{k})$.

According to Eqs. (23) and (24), the speed for $a(\mathbf{k})$ to approach the Gaussianity depends on the value of

$\eta(\mathbf{k})/n(\mathbf{k})$. Figure 7(a) shows the evolution of $\eta(\mathbf{k})/n(\mathbf{k})$ for $k = 1, 1.5, 3$ and 6 for $H_2 = 5 \times 10^{-6}$, and Fig. 7(b) shows the time-average, the maximum and the minimum of $\eta(\mathbf{k})/n(\mathbf{k})$ at each k during $100T_p$. These results are obtained by the numerical integration of the kinetic equation (17). For the initial spectrum (15c), $\eta(\mathbf{k})/n(\mathbf{k})$ is large in the range $2 \lesssim k \lesssim 3$. The wavenumber dependence of $\eta(\mathbf{k})/n(\mathbf{k})$ is consistent with the rapid growth of the fluctuation at $k = 3$ compared with those at the other wavenumbers observed in Fig. 5.

As shown in Fig. 1, the spectral variation for $H_2 = 5 \times 10^{-6}$ during $100T_p$ is not small. However, Fig. 7(b) indicates that the variation of the value of $\eta(\mathbf{k})/n(\mathbf{k})$ during $100T_p$ is almost constant in time except $1.5 < k < 3$, because the differences between the maximums and the minimums are small. Then, Eq. (24) suggests that $F^{(2)}(\mathbf{k})$ shows exponential decay in time. Figure 8 shows the evolution of $F^{(2)}$ of $k = 3$ for $H_2 = 5 \times 10^{-6}$ in DNS. It is found that the absolute value of $F^{(2)}$ exponentially decays as expected. When $F^{(2)}$ is fitted by an exponential function $-1/2 \exp(-\lambda(\mathbf{k})t)$, the decay rate $\lambda(\mathbf{k})$ obtained by the method of least squares is 2.58×10^{-3} . On the other hand, the decay rate predicted by RPA is $2\eta(\mathbf{k})/n(\mathbf{k})$. The time-average of $2\eta(\mathbf{k})/n(\mathbf{k})$ during

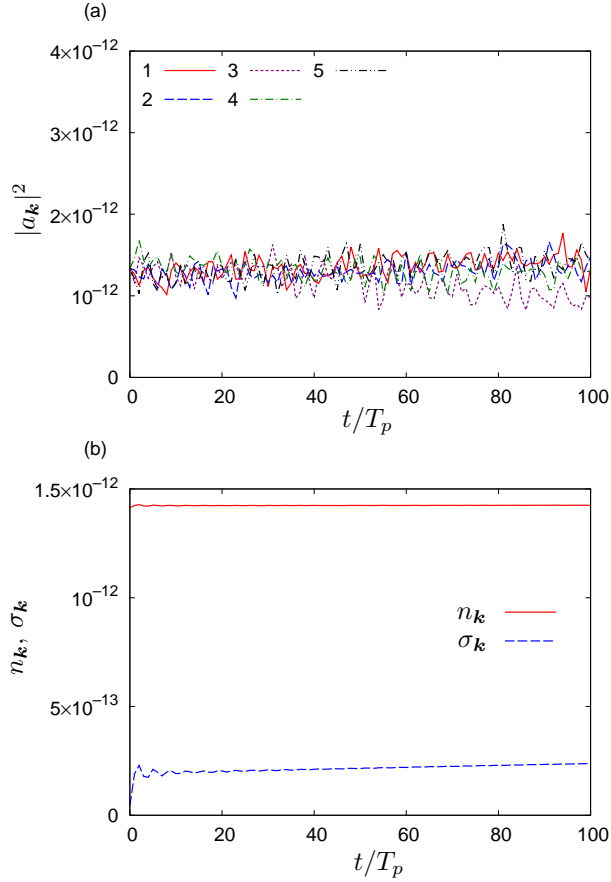


FIG. 6. (Color online) Evolution of the fluctuations of $|a_{\mathbf{k}}|^2$. $\omega = k^{1/2}$, $H_2 = 5 \times 10^{-6}$. (a): $|a_{\mathbf{k}}|^2$ in five independent realizations. $\mathbf{k} = (3, 0)$. (b): The mean $n_{\mathbf{k}}$ and the standard deviation $\sigma_{\mathbf{k}}$ of $|a_{\mathbf{k}}|^2$. $k = 3$.

$100T_p$ is 2.57×10^{-3} for $k = 3$. Thus the quantitative agreement between RPA and DNS is quite good.

Figure 9 shows the decay rate $\lambda(\mathbf{k})$ for $k = 1, 1.5, 3$ and 6 obtained by the least-square fit of the exponential function to $F^{(2)}(\mathbf{k})$ in DNS as a function of H_2 . It is observed that $\lambda(\mathbf{k})$ for each wavenumber is proportional to H_2 . As shown by Eqs. (17) and (24), RPA predicts that the time scales of the growth of the fluctuations as well as those of the evolution of the spectra are inversely proportional to the value of the Hamiltonian. It is consistent to the results shown in Fig. 9.

D. Moments for $p > 2$

The solution of Eq. (23) is given as

$$F^{(p)}(\mathbf{k}, t) = \sum_{j=2}^p C_j^{(p)} e^{-j\theta(\mathbf{k})},$$

$$\theta(\mathbf{k}) = \int_0^t \frac{\eta(\mathbf{k}, t')}{n(\mathbf{k}, t')} dt'. \quad (25)$$

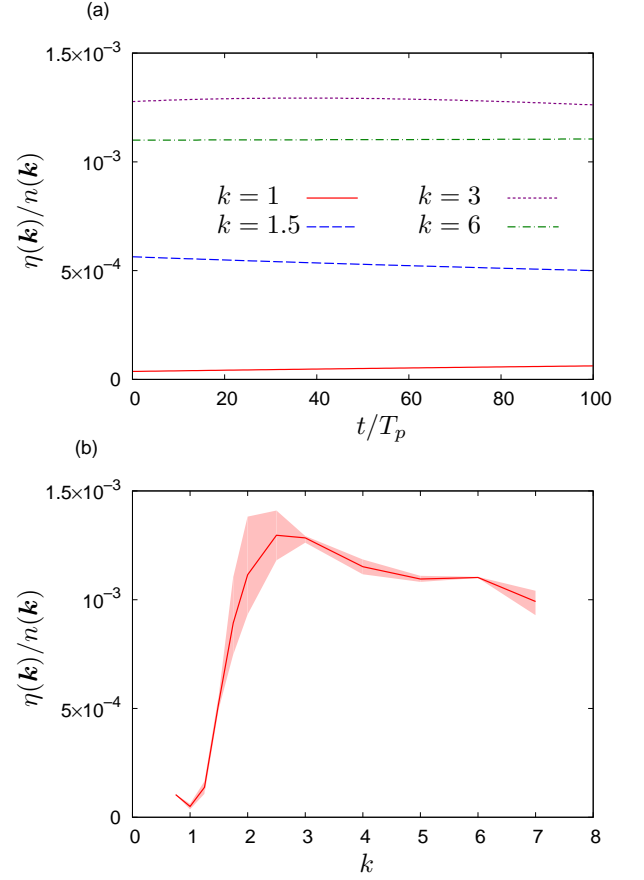


FIG. 7. (Color online) Value of $\eta(\mathbf{k})/n(\mathbf{k})$ for each wavenumber. $H_2 = 5 \times 10^{-6}$. (a): Evolution, (b): time-average, maximum and minimum during $0 \leq t \leq 100T_p$.

The coefficient $C_j^{(p)}$ is determined by the recurrence formula

$$C_j^{(p)} = \binom{p}{j} C_j^{(j)} \quad (j = 2, \dots, p-1),$$

$$C_2^{(2)} = F^{(2)}(\mathbf{k}, 0), \quad C_p^{(p)} = F^{(p)}(\mathbf{k}, 0) - \sum_{j=2}^{p-1} C_j^{(p)}, \quad (26)$$

where $\binom{p}{j}$ is the binomial coefficient [19].

The deviations from the Gaussianity $F^{(p)}$ at $k = 7$ at every $20T_p$ from $t = 0$ to $t = 100T_p$ for $H_2 = 5 \times 10^{-6}$ obtained by Eq. (25) and DNS are shown in Fig. 10 as functions of the order p of the moments. A large number of $a_{\mathbf{k}}$ is required to obtain reliable high-order moments. As explained before, to evaluate statistical quantities such as the moments of $a_{\mathbf{k}}$ at k , we use the values of $a_{\mathbf{k}'}$ in the annular domain $|k' - k| < 0.025$, hence the number of modes used in the statistical evaluation increases in proportion to k . This gives the reason to choose the large wavenumber $k = 7$ to evaluate the high-order moments. We confirmed that the tail of the probability density function of $|a_{\mathbf{k}}|^2$ defined below decays faster than

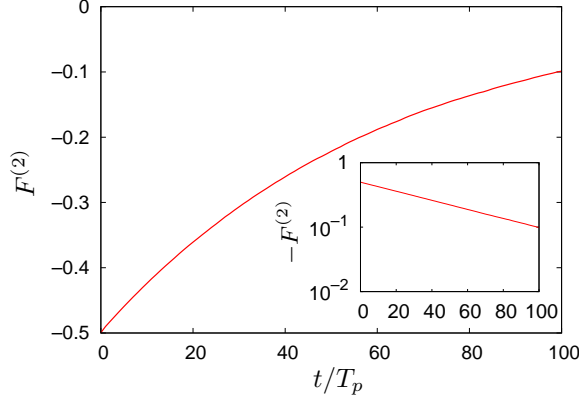


FIG. 8. (Color online) Evolution of $F^{(2)}$ in DNS. $H_2 = 5 \times 10^{-6}$, $k = 3$. The evolution is shown with the single logarithmic scale in the inset.

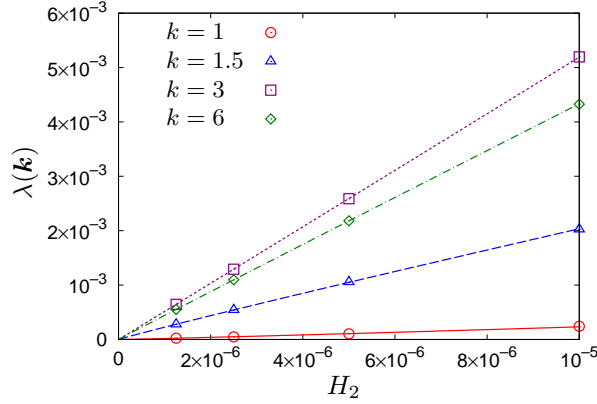


FIG. 9. (Color online) Dependence of the decay rate $\lambda(\mathbf{k})$ of $F^{(2)}(\mathbf{k})$ in DNS on H_2 .

the negative 9th power of $|a_{\mathbf{k}}|^2$. Therefore, the moments up to the 8th order are reliable. To obtain the deviation $F^{(p)}$ by Eq. (25) in RPA, $\theta(\mathbf{k})$ is approximated by $\theta(\mathbf{k}) \approx \overline{(\eta/n)}t$, where $\overline{(\eta/n)}$ is the time-averaged value of $\eta(\mathbf{k})/n(\mathbf{k})$ during $100T_p$. Similarly, the evolution of the deviations $F^{(p)}$ at $k = 7$ obtained by DNS and RPA are compared in Fig. 11. Even though the value of $\theta(\mathbf{k})$ is approximated by $\overline{(\eta/n)}t$ and the high-order moments such as of 8th-order are treated, RPA and DNS show another good agreement.

E. Evolution of Distribution of Amplitude Fluctuations

RPA also gives the evolution of the probability density function (PDF) $\mathcal{P}(s(\mathbf{k}))$ of $s(\mathbf{k})$, which is a stochastic

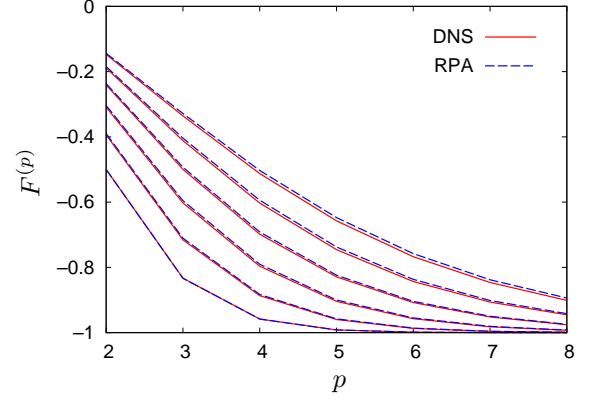


FIG. 10. (Color online) Comparison of $F^{(p)}$ between DNS and RPA for each p . $t = 0, 20T_p, \dots, 100T_p$ from bottom to top. $H_2 = 5 \times 10^{-6}$, $k = 7$.

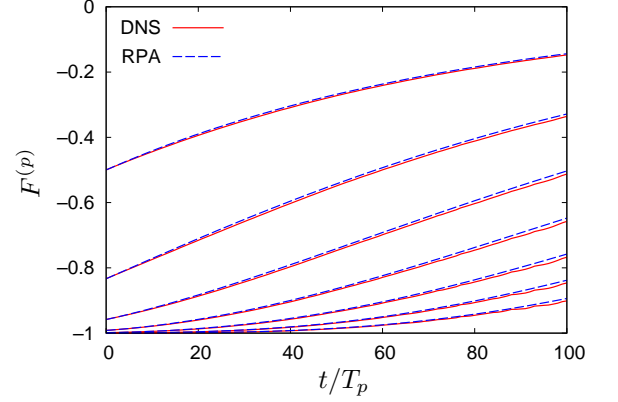


FIG. 11. (Color online) Evolution of $F^{(p)}$ in DNS and RPA. $p = 2, 3, \dots, 8$ from top to bottom. $H_2 = 5 \times 10^{-6}$, $k = 7$.

variable defined by $s(\mathbf{k}) = |a(\mathbf{k})|^2/\delta(\mathbf{0})$, as follows [14]:

$$\frac{\partial \mathcal{P}(s(\mathbf{k}))}{\partial t} = \frac{\partial \mathcal{F}(\mathbf{k})}{\partial s(\mathbf{k})},$$

$$\mathcal{F}(\mathbf{k}) = s(\mathbf{k}) \left(\gamma(\mathbf{k}) \mathcal{P}(s(\mathbf{k})) + \eta(\mathbf{k}) \frac{\partial \mathcal{P}(s(\mathbf{k}))}{\partial s(\mathbf{k})} \right), \quad (27)$$

where $\eta(\mathbf{k})$ and $\gamma(\mathbf{k})$ are the coefficients (17b) and (17c) in the kinetic equation (17). The PDF $\mathcal{P}(s)$ at $k = 3$ for four values of H_2 is shown in Fig. 12. The PDF is obtained by the numerical integration of Eq. (27) until $100T_p$. Figure 12 has s normalized by its initial value $n(0)$, i.e., $x = s/n(0)$ on the abscissa. The variation of $\mathcal{P}(x)$ is faster for larger H_2 . For $H_2 = 1.25 \times 10^{-6}$, $\mathcal{P}(x)$ has a narrow distribution with a remnant of the initial distribution $\delta(x - 1)$ even at $= 100T_p$, while for $H_2 = 1 \times 10^{-5}$, it has almost reached the χ^2 -distribution with 2 degrees of freedom corresponding to the Gaussianity of $a(\mathbf{k})$ by the same time. The PDF obtained in DNS at $100T_p$ is also shown in Fig. 12. For all H_2 , the theoretical prediction of RPA and the result of DNS agree quite well. RPA does not rely on any proximity to the Gaussianity

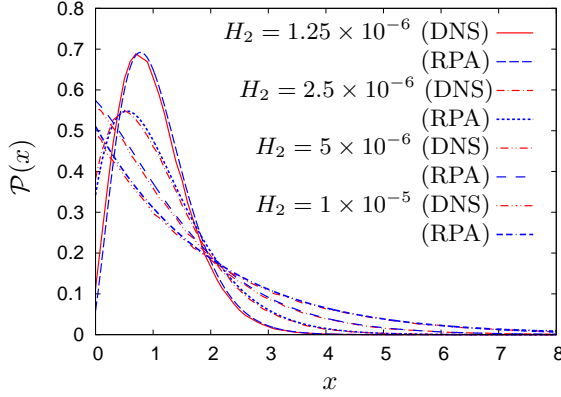


FIG. 12. (Color online) Comparison of $\mathcal{P}(x)$ in DNS and RPA. $k = 3$, $t = 100T_p$.

of $a_{\mathbf{k}}$ [12]. Figures 10, 11 and 12 confirm the validity of RPA even when the Gaussianity of $a_{\mathbf{k}}$ has not been established at all.

The coefficients $\eta(\mathbf{k})$ and $\gamma(\mathbf{k})$ in Eq. (27) vary as the wave action $n(\mathbf{k})$ evolves. Then, in the calculation of Eq. (27), the calculation of the kinetic equation (17a) is first performed to obtain $\gamma(\mathbf{k}, t)$ and $\eta(\mathbf{k}, t)$ as functions of time. Moreover, since $s(\mathbf{k})$ does not have fluctuations initially in this study, $\mathcal{P}(x, 0) = \delta(x - 1)$ should be employed for the initial condition to numerically obtain $\mathcal{P}(s)$ at later time according to Eq. (27). However, it causes numerical difficulty. If $\mathcal{P}(x)$ is very narrow, the diffusion term is dominant in the right-hand side of Eq. (27). Then, in the very early stage of the evolution, Eq. (27) can be approximated by the diffusion equation

$$\frac{\partial \mathcal{P}(x)}{\partial t} = \mu \frac{\partial^2 \mathcal{P}(x)}{\partial x^2}, \quad \mu = \frac{x_0 \eta_0}{n_0}, \quad x_0 = 1, \quad (28)$$

where η_0 is η at $t = 0$. This makes it possible that the original initial condition $\mathcal{P}(x, 0) = \delta(x - 1)$ is replaced by the state after the PDF evolves according to Eq. (28) for small time t_0 , i.e., the normal distribution with small standard deviation σ_0

$$\mathcal{P}(x, t_0) = \frac{1}{\sqrt{2\pi}\sigma_0} \exp\left(-\frac{(x-1)^2}{2\sigma_0^2}\right), \quad (t_0 = \sigma_0^2/2\mu) \quad (29)$$

to numerically solve the initial-value problem of Eq. (27). For the result in Fig. 12, $\sigma_0 = 0.1$ is used. Even if $\sigma_0 = 0.05$ is used, perceptible change in Fig. 12 is not produced. To obtain $\mathcal{P}(x)$ at $k = 3$ in DNS, $s_{\mathbf{k}}$ of 1,680 modes in the annular domain $|k - 3| < 0.025$ are used. Since 256 realizations in DNS are independently performed, $430,080 (= 1,680 \times 256)$ data is used to draw $\mathcal{P}(x)$ in Fig. 12.

IV. CONCLUDING REMARK

In this work, direct numerical simulations (DNS) for a three-wave resonant Hamiltonian system are performed, and the validity of the Random Phase and Amplitude Formalism (RPA) recently proposed in the weak turbulence is evaluated by quantitative comparison with DNS. It is confirmed that the theoretical prediction of RPA and the result of DNS agree quite well in all the statistical aspects of the amplitude fluctuations such as the high-order moments and the evolution of the probability density function (PDF) of $s(\mathbf{k}) = |a(\mathbf{k})|^2/\delta(\mathbf{0})$ of each mode, the asymptotic approach of $a(\mathbf{k})$ to the Gaussianity and its time scales, and so on. We have performed the comparison between RPA and DNS for the same three-wave model but in the case of an anisotropic initial spectrum, and obtained the same level of agreement between RPA and DNS. (Not shown here)

The comparison is restricted to the three-wave resonant system in this work. In RPA for four-wave systems, there exist some characteristics which the three-wave systems do not have such as the renormalization of the nonlinear frequency. Hence, the comparison for four-wave systems are still necessary. The authors numerically investigated the growth of the amplitude fluctuations in a four-wave system [20]. It was found that the time scales of the growth of the fluctuations is much shorter than those of the spectral variations in the large wavenumbers away from the spectral peak. Although we did not attempt quantitative comparison with RPA at that time, we felt suspicion about the validity of RPA because RPA predicts that both time scales should be of the same order in terms of the amplitude expansion or in terms of the Hamiltonian H . This suspicion was actually one of the motives of the present work. Judging from the complete agreement between RPA and DNS regarding to a three-wave system reported here, we expect that this suspicion which we previously felt about the validity of RPA would be cleared up when we will have finished the same kind of comparison between RPA and DNS for some four-wave systems as well. In Ref. [20], we also investigated statistical nature of $ds(\mathbf{k})/dt$ by DNS. We numerically showed that the fluctuation of $ds(\mathbf{k})/dt$ approaches a quasi-steady state faster than $s(\mathbf{k})$ and analytically showed that PDF of $ds(\mathbf{k})/dt$ has the Laplace distribution. No work for $ds(\mathbf{k})/dt$ were found in the framework of RPA. This is also one of our future work.

RPA gives theoretical prediction about the multi-mode statistics such as the joint probability density $P^{(N)}$ of $|a_{\mathbf{k}_1}|^2, \dots, |a_{\mathbf{k}_N}|^2$ as well as the single-mode statistics [21], but we have restricted our attention in the present study only to the single-mode statistics and have not treated those multi-mode statistics at all. With regard to the multi-mode statistics, it is pointed out that the original results by RPA are not correct [15]. Then, numerical investigation of the multi-mode statistics remains to be done.

Our present numerical results also prompt a new ques-

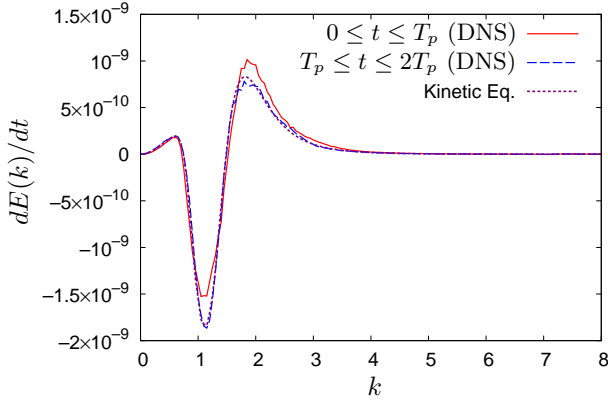


FIG. 13. (Color online) Comparison of $dE(k)/dt$ obtained from the spectral variation during one period in DNS and from kinetic equation.

tion of the time scales which is required by the weak turbulence theory. Janssen [22] derived a kinetic equation in a different form from that by Hasselmann [1] and by Zakharov *et al.* [11]. He pointed out that the conventional kinetic equation is recovered by replacing the “resonance function”

$$R_i(\Delta\omega, t) = \frac{\sin(\Delta\omega t)}{\Delta\omega}, \quad (30)$$

by the delta function which is the asymptotic of R_i in the limit $t \rightarrow \infty$. He claimed that non-resonant interactions as well as resonant interactions contribute the spectral evolution until the time when the replacement is validated. In RPA investigated here, the important equations such as for the moments Eq. (20) and for the

PDF Eq. (27) are derived. It is based on the premise that the linear time scale $\tau_l = O(2\pi/\omega)$ and the nonlinear time scale, i.e., the time scale of the spectral evolution $\tau_n = O(1/(\epsilon^2\omega))$ are well separated, and the intermediate time scale

$$\tau_l \ll \tau_i \ll \tau_n, \quad (31)$$

should exist. Based on their derivation, the equations in RPA are supposed to describe the time rate of change of the moments and the PDF in the time scale of τ_i .

In Fig. 13, the time rates of spectral changes $dE(k)/dt$ during T_p from $t = 0$ to $t = T_p$ and from $t = T_p$ to $t = 2T_p$ for $H_2 = 5 \times 10^{-6}$ are compared with that obtained by the kinetic equation (17) for the initial spectrum. Although the time rate of the spectral change for the first T_p is slightly different from the prediction of the kinetic equation, the rate during the period T_p from $t = T_p$ to $t = 2T_p$ almost perfectly coincides with the prediction of the kinetic equation. The time rates of change of the higher-order moments during T_p also show similar agreements between DNS and RPA. These agreements between DNS and RPA in the short-time evolution appears to contradict the procedure of the derivation of the statistical equations in RPA. This short-time agreement has already been pointed out previously [23]. This might affect the basis of the weak turbulence theory including RPA, and must be investigated further.

ACKNOWLEDGMENTS

The authors are grateful to Dr. Yuri V. Lvov and Dr. Yeontaek Choi for valuable discussions. The numerical simulations are performed at Information Technology Center, Nagoya University.

-
- [1] K. Hasselmann, *J. Fluid Mech.* **12**, 481 (1962).
 - [2] V. E. Zakharov and N. N. Filonenko, *Sov. Phys. Dokl.* **10**, 881 (1967).
 - [3] Y. Lvov, S. Nazarenko, and R. West, *Physica D* **184**, 333 (2003).
 - [4] C. Connaughton, S. Nazarenko, and A. C. Newell, *Physica D* **184**, 86 (2003).
 - [5] E. Kartashova, *Nonlinear resonance analysis: theory, computation, applications* (Cambridge Univ. Pr., 2010).
 - [6] A. C. Newell, S. Nazarenko, and L. Biven, *Physica D* **152–153**, 520 (2001).
 - [7] S. Dyachenko, A. C. Newell, A. Pushkarev, and V. E. Zakharov, *Physica D* **57**, 96 (1992).
 - [8] A. C. Newell and B. Rumpf, *Annu. Rev. Fluid Mech.* **43**, 59 (2011).
 - [9] A. N. Pushkarev, *Eur. J. Mech. B/Fluids* **18**, 345 (1999).
 - [10] G. Düring, C. Josserand, and S. Rica, *Phys. Rev. Lett.* **97**, 025503 (2006).
 - [11] V. E. Zakharov, V. S. L’vov, and G. Falkovich, *Kolmogorov Spectra of Turbulence I* (Springer-Verlag, Berlin, 1992).
 - [12] Y. V. Lvov and S. Nazarenko, *Phys. Rev. E* **69**, 66608 (2004).
 - [13] S. Nazarenko, *Wave Turbulence* (Springer, Heidelberg, 2011).
 - [14] Y. Choi, Y. V. Lvov, S. Nazarenko, and B. Pokorni, *Phys. Lett. A* **339**, 361 (2005).
 - [15] G. L. Eyink and Y.-K. Shi, *Physica D* **241**, 1487 (2012).
 - [16] D. J. Benney and A. C. Newell, *Stud. Appl. Math* **48**, 29 (1969).
 - [17] D. J. Benney and P. G. Saffman, *Proc. R. Soc. A* **289**, 301 (1966).
 - [18] C. Canuto, M. Y. Hussaini, A. Quarteroni, and T. A. Zang, *Spectral Methods in Fluid Dynamics* (Springer-Verlag, 1988).
 - [19] The explicit expression of the solution of Eq. (23) in Ref. [12] is incorrect.
 - [20] M. Tanaka and N. Yokoyama, *Physica D* **240**, 1145 (2011).
 - [21] Y. Choi, Y. V. Lvov, and S. Nazarenko, *Physica D* **201**,

121 (2005).

[22] P. A. E. M. Janssen, *J. Phys. Oceanogr.* **33**, 863 (2003).

[23] M. Tanaka, *J. Phys. Oceanogr.* **37**, 1022 (2007).